

FILM: Frame Interpolation for Large Motion

Fitsum Reda Janne Kontkanen Eric Tabellion Deqing Sun
Caroline Pantofaru Brian Curless
Google Research

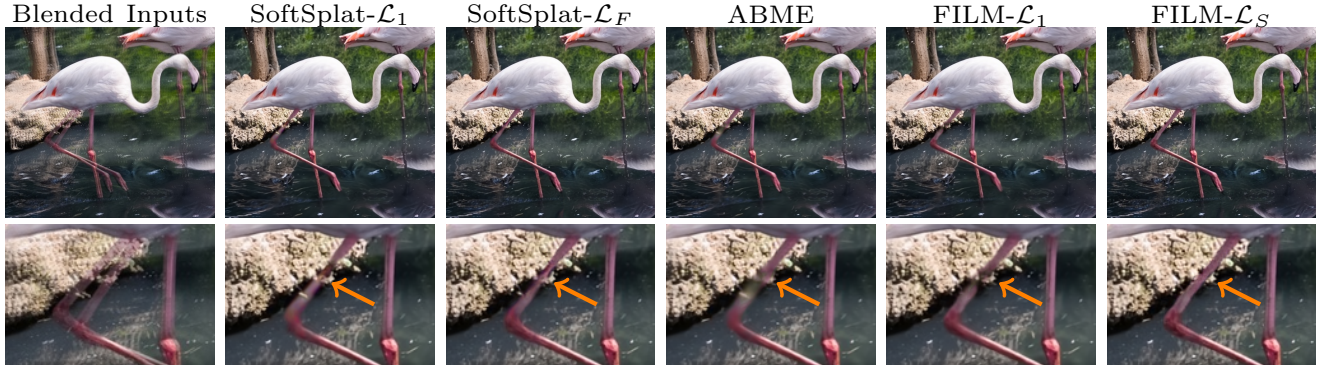


Figure 1. Frame interpolation example from DAVIS-dataset [27] featuring a walking flamingo. From left to right: The input frames overlaid, SoftSplat- \mathcal{L}_1 [21], SoftSplat- \mathcal{L}_F [21], ABME [26], our FILM- \mathcal{L}_1 , and our FILM- \mathcal{L}_S . FILM- \mathcal{L}_S produces crisp frame, while color distortions and transparencies can be seen in ABME and SoftSplat, respectively. SoftSplat renderings are generated from our faithful implementations, which we found to be quite comparable to the original paper, see Section 5.2.

Abstract

We present a frame interpolation algorithm that synthesizes multiple intermediate frames from two input images with large in-between motion. Recent methods use multiple networks to estimate optical flow or depth and a separate network dedicated to frame synthesis. This is often complex and requires scarce optical flow or depth ground-truth. In this work, we present a single unified network, distinguished by a multi-scale feature extractor that shares weights at all scales, and is trainable from frames alone. To synthesize crisp and pleasing frames, we propose to optimize our network with the Gram matrix loss that measures the correlation difference between feature maps. Our approach outperforms state-of-the-art methods on the Xiph large motion benchmark. We also achieve higher scores on Vimeo-90K, Middlebury and UCF101, when comparing to methods that use perceptual losses. We study the effect of weight sharing and of training with datasets of increasing motion range. Finally, we demonstrate our model’s effectiveness in synthesizing high quality and temporally coherent videos on a challenging near-duplicate photos dataset. Codes and pre-trained models are available at <https://github.com/google-research/frame-interpolation>.

1. Introduction

Frame interpolation – synthesizing intermediate images between a pair of input frames – is an important practical problem with increasing reach. Modern TVs have dedicated hardware to up-sample the incoming frame rate, so that relatively low frame-rate broadcasts can be displayed smoothly on high frame-rate displays. Further, frame interpolators can synthesize slow-motion video from regular frame rate footage, with increasingly impressive results powered by rapid progress in deep neural networks.

Recently, a new use case has emerged. Digital photography, especially with the advent of smartphones, has made it effortless to take several pictures within a few seconds, and people naturally do so often, in their quest for just the right photo that captures the moment. These “near duplicates” create an exciting opportunity: interpolating between them can lead to surprisingly engaging videos that reveal scene (and some camera) motion, often delivering an even more pleasing sense of the moment than any one of the original photos.

A major challenge in frame interpolation, for frame-rate up-sampling and especially for near-duplicate photo interpolation (for which the temporal spacing can be a second or more), is handling large scene motion effectively. In our work, we propose a new approach for doing just that, out-

performing the state of the art. To give some context, we discuss progress in the area of frame interpolation and then summarize our approach and contributions.

Recently, impressive interpolations have been achieved using multiple networks. In particular, the DAIN approach [2] incorporates a depth network to handle pixel occlusions well, and [21, 26] add motion estimation networks to robustly estimate pixel-wise motion. Each prior-network needs its own scarce depth, optical flow, or additional training samples. However, this increases the complexity of the pre-training and fine-tuning procedures, as well as the computational complexity.

Our other observation is that, while the state-of-the-art approaches score well on benchmarks [1, 18, 40], we found them to be sub-optimal in large motion interpolation. First, interpolated frames appear blurry, especially when trained with color losses. Second, at test time, models perform well when the motion range matches that of the training datasets', but generalize poorly on more extreme motion. One could approach this with data that captures the desired range [32]. We instead propose a network that generalizes well in small and large motion.

In this work, we present a unified, single-stage, network for frame interpolation of large motion (FILM), trained from frames alone. FILM adopts a multi-scale feature extractor [37], that shares weights at different scales, for feature pyramid construction and bi-directional motion estimation. It builds upon the intuition that large motion at finer scales should be similar to small motion at coarser scales.

Recent optical flow research also shows this benefit [9, 10] in improving generalization of models from small to large motion. We show in Section 5 the effectiveness of our approach in handling large motion. We also study the impact of the training dataset's motion range distribution on test-time performance, and show still further improvements achieved by training on large motion datasets.

Further, to improve the realism and sharpness of interpolated frames, we propose to optimize FILM with the Gram Matrix loss [8], which matches the *auto-correlation* of the high-level VGG features.

The main contributions of our work are:

- A unified, single-stage, model for large motion frame interpolation.
- A scale-agnostic bi-directional motion estimation module with a multi-scale feature extractor that shares the same weights at each pyramid-scale.
- Using the Gram matrix loss to generate crisp and pleasing intermediate frames.

2. Related Work

Since the resurgence of deep neural networks, various CNN-based algorithms [2, 6, 11, 15, 20–26, 39] propose to

train frame interpolators by supervising with ground-truth frames [4]. Other works [17, 29] propose to learn in an un-paired manner to alleviate the need for high frame-rate training data. Common algorithmic approaches are (1) direct generation of frames from the inputs [12, 36], or (2) re-sampling the inputs based on learned flows [11, 18] or kernels [23]. Ours is a hybrid approach, where we learn a bi-directional flow and a feature pyramid from the inputs; and the final frame is synthesized by conditioning on the warped feature pyramid.

Single-Stage Networks. The first CNN-based frame interpolators propose UNet-like networks, trained from inputs and target frames [11, 18]. Recent work [2] introduces depth estimation modules to handle pixel occlusions, and work in [21, 26] incorporates motion estimation modules [25, 34]. While impressive results are achieved, multiple networks can make training processes complex or increase computational complexity. Our work introduces a single unified network, trainable from frame triples alone, without additional priors, and achieves state-of-the-art results.

Large Motion. Handling large motion is an important yet under-explored topic in frame interpolation. The work in [32] handles large motion by training on 4K sequences with extreme motion. While this is a viable approach, it does not generalize well on regular footage as discussed in [26]. Similarly, other approaches [21, 26] perform poorly when the test motion range deviates from the training motion range. We adopt a multi-scale shared feature extractor module [9, 10, 37] that allows us to learn large and small motion with equal priority, and show favorable generalization ability in various benchmarks.

Image Quality. One of our key contributions is high quality frame synthesis. Prior work [22–24] improves image quality by learning a per-pixel kernel instead of an offset vector, which is then convolved with the inputs. While effective at improving quality, the method cannot handle large motion well. Other approaches optimize models with perceptual losses [21, 23]. Some consider an adversarial loss [38], albeit with a complex training process. Our work proposes to adopt the Gram matrix loss [8], which builds up on the perceptual loss and yields high quality frames, especially when inpainting large dis-occlusions.

3. Method

Given two input frames $(\mathbf{I}_0, \mathbf{I}_1)$, we synthesize a mid-frame $\hat{\mathbf{I}}_t$, with time $t \in (0, 1)$, as:

$$\hat{\mathbf{I}}_t = \mathcal{M}(\mathbf{I}_0, \mathbf{I}_1), \quad (1)$$

where \mathcal{M} is our FILM network trained with a ground-truth \mathbf{I}_t . During training, we supervise at $t = 0.5$ and we predict more in-between frames by recursively invoking FILM.

FILM has three main stages: Scale-agnostic feature extraction, motion estimation, and a fusion stage that outputs the resulting color image. Figure 2 shows an overview of FILM.

Feature extraction. In contrast to other frame interpolation methods, we use a scale-agnostic feature extractor adapted from multi-view image fusion [37]. The unique aspect of this feature extractor is that it enables weight sharing in the flow prediction stage that follows, simultaneously learning shared weights on coarse and fine resolutions. It is constructed in three steps as follows.

First, we create image pyramids $\{\mathbf{I}_0^l\}$ and $\{\mathbf{I}_1^l\}$ for the two inputs, where $l \in [1, 7]$ is the pyramid level.

Second, starting at the image at each l -th pyramid level, we build feature pyramids (the columns in Figure 2) using a shared UNet encoder. Specifically, we extract multi-scale features $\{\mathbf{f}_0^{l,d}\}$ and $\{\mathbf{f}_1^{l,d}\}$, with $d \in [1, 4]$ being the depth at that l -th level (Figure 2 only uses $d \in [1, 3]$ for illustration). Mathematically,

$$\mathbf{f}_0^{l,d} = \mathcal{H}^d(\mathbf{I}_0^l), \quad (2)$$

where \mathcal{H}^d is a stack of convolutions, shown in Figure 2 with the green arrow for $d=1$, red for $d=2$, and dark-blue for $d=3$. Note that, the same $\theta^{(\mathcal{H}^d)}$ convolution weights are shared for the same d -th depth at each pyramid level, to create *compatible multiscale features*. Each \mathcal{H}^d is followed by an average pooling with a size and stride of 2.

As a third and final step of our feature extractor, we construct our scale-agnostic feature pyramids, $\{\mathbf{F}_0^l\}$ and $\{\mathbf{F}_1^l\}$, by concatenating the feature maps with different depths, but the same spatial dimensions, as:

$$\mathbf{F}_0^l = (\mathbf{f}_0^{l-2,d=3}, \mathbf{f}_0^{l-1,d=2}, \mathbf{f}_0^{l,d=1}), \quad (3)$$

and the scale-agnostic feature, \mathbf{F}_1^l of \mathbf{I}_1 , at the l -th pyramid level, can be given in a similar way by Equation 3. As shown in Figure 2, the finest level feature (green) can only aggregate one feature map, the second finest level two (green+red), and the rest can aggregate three shared feature maps.

Flow Estimation. Once we extract the feature pyramids, $\{\mathbf{F}_0^l\}$ and $\{\mathbf{F}_1^l\}$, we use them to calculate a bi-directional motion at each pyramid level. Similar to [34], we start the motion estimation from the coarsest level (in our case $l = 7$). However, in contrast to other methods, we directly predict task oriented [40] flows, $\mathbf{W}_{t \rightarrow 0}$ and $\mathbf{W}_{t \rightarrow 1}$, from the mid-frame to the inputs.

Predicting optical flow from yet-to-be-computed mid-frame \mathbf{I}_t would not be possible if we were to supervise by ground truth optical flow between the input frames, but in an end-to-end frame interpolation system, the network is actually well positioned to do this just based on the input frames and their corresponding feature pyramids.

We compute the task oriented flow at each level as a sum of predicted residual and the upsampled flow from the coarser level. Flow at each level $\mathbf{W}_{t \rightarrow 1}^l$ is predicted as a residual over the coarser level $l + 1$ as:

$$\mathbf{W}_{t \rightarrow 1}^l = (\mathbf{W}_{t \rightarrow 1}^{l+1})_{\times 2} + \mathcal{G}^l(\mathbf{F}_0^l, \hat{\mathbf{F}}_{t \leftarrow 1}^l), \quad (4)$$

where $(\bullet)_{\times 2}$ is a 2D bilinear up-sampling operation, \mathcal{G}^l is a stack of convolutions that calculates the per-pixel residual vector, and $\hat{\mathbf{F}}_{t \leftarrow 1}^l$ is the backward warped scale-agnostic feature map at $t=1$, obtained by bilinearly warping \mathbf{F}_1^l with the upsampled flow estimate, as,

$$\hat{\mathbf{F}}_{t \leftarrow 1}^l = \mathcal{T}(\mathbf{F}_1^l, (\mathbf{W}_{t \rightarrow 1}^{l+1})_{\times 2}), \quad (5)$$

with \mathcal{T} being a bilinear resample (warp) operation. Figure 2 depicts \mathcal{G}^l by the blue or white arrows, depending on the pyramid level.

Finally, we create the feature pyramid at the intermediate time t , $\{\mathbf{F}_{t \leftarrow 1}^l\}$ and $\{\mathbf{F}_{t \leftarrow 0}^l\}$, by backward warping the feature pyramid, at $t=1$ and $t=0$, with the flows given by Equation 4, as:

$$\mathbf{F}_{t \leftarrow 1}^l = \mathcal{T}((\mathbf{F}_1^l, \mathbf{I}_1^l), \mathbf{W}_{t \rightarrow 1}^l), \quad (6)$$

$\mathbf{F}_{t \leftarrow 0}^l$ can be given in a similar way as Equation 6.

Fusion. The final stage of FILM concatenates, at each l -th pyramid, the scale-agnostic feature maps at t and the bi-directional motions to t , which are then fed to a UNet-like [30] decoder to synthesize the final mid-frame $\hat{\mathbf{I}}_t$. Mathematically, the fused input at each l -th decoder level is given by,

$$(\mathbf{F}_{t \leftarrow 1}^l, \mathbf{F}_{t \leftarrow 0}^l, \mathbf{W}_{t \rightarrow 0}^l, \mathbf{W}_{t \rightarrow 1}^l). \quad (7)$$

Figure 2 illustrates the decoder’s convolutions and resulting activations with a white arrow and gray boxes, respectively.

3.1. Loss Functions

We use only image synthesis losses to supervise the final output of our FILM network; we do not use auxiliary losses tapped into any intermediate stages. Our image synthesis loss is a combination of three terms.

First, we use the L1 reconstruction loss that minimizes the pixel-wise RGB difference between the interpolated frame $\hat{\mathbf{I}}_t$ and the ground-truth frame \mathbf{I}_t , given by:

$$\mathcal{L}_1 = \|\hat{\mathbf{I}}_t - \mathbf{I}_t\|_1. \quad (8)$$

The \mathcal{L}_1 loss allows our FILM network to capture the motion between the inputs $(\mathbf{I}_0, \mathbf{I}_1)$ and is proved to yield interpolation results that score well on benchmarks, as is shown

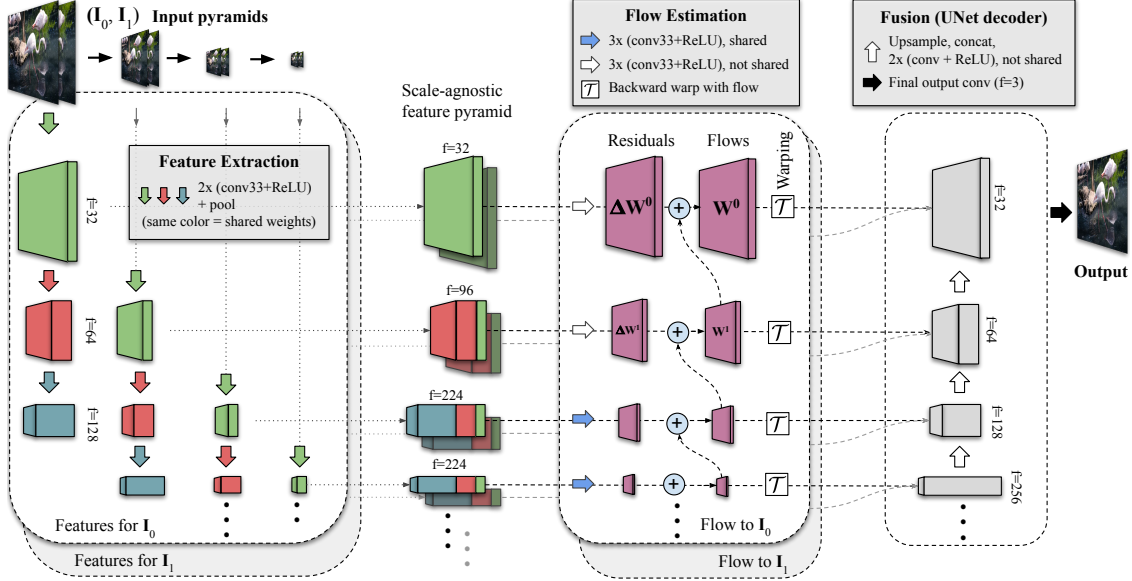


Figure 2. FILM architecture overview. Our feature extractor, adopted from [37], produces “scale agnostic” features that have similar meaning across scales.

in Section 5.2. However, the interpolated frames are often blurry. We also found this to be the case for the other methods trained with similar losses.

Second, to enhance image details, we add a perceptual loss, using the L1 norm of the VGG-19 high-level feature representation [33]. Mathematically, the perceptual loss, also called VGG-loss, \mathcal{L}_{VGG} , is given by,

$$\mathcal{L}_{\text{VGG}} = \frac{1}{L} \sum_{l=1}^L \alpha_l \left\| \Psi_l(\hat{\mathbf{I}}_t) - \Psi_l(\mathbf{I}_t) \right\|_1, \quad (9)$$

where $\Psi_l(\mathbf{I}_i) \in \mathbb{R}^{H \times W \times C}$ is the feature map from the l -th selected layer of a pre-trained Imagenet VGG-19 network for $\mathbf{I}_i \in \mathbb{R}^{H \times W \times 3}$, L is the number of the finer layers considered, and α_l is an importance weight of the l -th layer. Due to the receptive fields of each layer, the perceptual loss enforces structural similarity over a small neighborhood around each output pixel, and is proven to help in reducing blurry artifacts in various image synthesis tasks [7, 8, 14, 23, 31].

Finally, we employ the Style loss [8, 16, 28] to further expand on the benefits of \mathcal{L}_{VGG} . The style loss $\mathcal{L}_{\text{Gram}}$, also called Gram matrix loss, is the L2 norm of the auto-correlation of the VGG-19 high-level feature representations [33]:

$$\mathcal{L}_{\text{Gram}} = \frac{1}{L} \sum_{l=1}^L \alpha_l \left\| \mathbf{M}_l(\hat{\mathbf{I}}_t) - \mathbf{M}_l(\mathbf{I}_t) \right\|_2, \quad (10)$$

where the Gram matrix of the interpolated frame at the l -th layer, $\mathbf{M}_l(\hat{\mathbf{I}}_t) \in \mathbb{R}^{C \times C}$, is given by:

$$\mathbf{M}_l(\hat{\mathbf{I}}_t) = (\Psi_l(\hat{\mathbf{I}}_t))^T (\Psi_l(\hat{\mathbf{I}}_t)), \quad (11)$$

and the Gram matrix of the ground-truth image, $\mathbf{M}_l(\mathbf{I}_t)$, can be given in a similar way as Equation 11.

To the best of our knowledge, this is the first work that applies the Gram matrix loss for the task of frame interpolation. We found this loss to be effective in resolving image sharpness as well as preserving image details when inpainting disocclusions in sequences with large motion. For both \mathcal{L}_{VGG} and $\mathcal{L}_{\text{Gram}}$, we use five activations from the VGG-19 layers, namely `relu1_2`, `relu2_2`, `relu3_2`, `relu4_2`, `relu5_2`, with a weight of 0.3846, 0.2083, 0.2703, 0.1786, 6.667, respectively.

To achieve high benchmark scores as well as high quality intermediate frame synthesis, we train our models with an optimally weighted combination of the RGB, VGG and Gram matrix losses. The combined loss, which we denote \mathcal{L}_S , is defined as,

$$\mathcal{L}_S = w_l \mathcal{L}_1 + w_{\text{VGG}} \mathcal{L}_{\text{VGG}} + w_{\text{Gram}} \mathcal{L}_{\text{Gram}}, \quad (12)$$

with the weights $(w_l, w_{\text{VGG}}, w_{\text{Gram}})$ determined empirically, as detailed in Section 4.

3.2. Large Motion Datasets

To study FILM’s ability to handle large motion, we created a “bracketed” dataset containing five training sub-sets. Each containing examples with motion disparity in the following ranges, in pixels: 0-40, 0-60, 0-80, 0-100, and 0-120.

We procedurally mine 512×512 image triplets from publicly available videos, extending the method described in [5]. First, we track image features over several consecutive frames in each video, using sparse optical flow fea-

ture tracking [35]. Next, we consider several candidate image triplets and compute the distribution of features’ motion disparity for each candidate. Finally, we retain an image triplet if its distribution statistics are within the considered bracket’s motion lower and upper bound.

We apply this procedure to generate several motion brackets, with lower and upper motion bound increasing by 20 pixels, i.e.: 0-20, 20-40, ..., 100-120. The motion distribution histograms of these brackets are shown overlapped in Figure 3. This method allows us to blend brackets together in equal proportions, to construct training datasets with the following motion ranges: 0-40, 0-60, ..., 0-120. The effect of training using blends with increasing motion range is analyzed in Section 5.3.

4. Implementation Details

We implemented our model in TensorFlow 2. As training data, we use either Vimeo-90K or one of our large motion datasets described in Section 3.2.

For the Vimeo-90K dataset, each mini-batch contains 256×256 randomly cropped frame triplets in the range $[0, 1]$, with the middle being the ground-truth, for a $t=0.5$ interpolation. We use a batch size of 8 distributed over 8V100 GPUs. To combat over-fitting, we apply data augmentation: Random rotation with $[-45^\circ, 45^\circ]$, rotation by multiples of 90° , horizontal flip, and reversing triplets order. We optimize our model with Adam [13] using $\beta_1=0.9$ and $\beta_2=0.999$, without weight decay. We use an initial learning rate of $1e^{-4}$ scheduled with exponential decay rate of 0.464, and decay steps of 750K, in a stair-wise manner, for a total of 3M iterations.

For comparison with the recent state-of-the-art models, we trained two versions: One optimized using \mathcal{L}_1 loss alone, which achieves higher benchmark scores, and another, that favours image quality, trained with our proposed style loss, \mathcal{L}_S . Our style loss optimally combines \mathcal{L}_1 , \mathcal{L}_{VGG} , and \mathcal{L}_{Gram} . We use a piecewise linear weight-schedule to select a weight for each loss at each iteration. Specifically, we assign weights of $(1.0, 1.0, 0.0)$ for 1.5M iterations, and weights of $(1.0, 0.25, 40.0)$ for the last 1.5M iterations. All hyper-parameters were obtained using grid search with a light-weight version of our model, for computational tractability.

To perform our qualitative evaluations, we also implement the SoftSplat [21] in TensorFlow 2, since pre-trained models were not available at the time of writing. In Figure 1, we show our faithful implementations on a DAVIS [27] image sample rendered in [21]. We found that renderings with our implementation are comparable to the ones provided in the original paper.

5. Results

In this section, we quantitatively and qualitatively evaluate our FILM network. We additionally compare FILM with the recent state-of-the-art algorithms, including DAIN [2], AdaCoF [15], BMBC [25], SoftSplat [21], and ABME [26].

Datasets. We report quantitative metrics on widely used datasets, including Vimeo-90K [40], UCF101 [18] Middlebury [1], and on a recently introduced large-motion dataset Xiph [19]. We use the Vimeo-90K as the training dataset for all methods when conducting both qualitative and quantitative comparisons. We evaluate the visual quality of interpolated frames on a new challenging near-duplicate photos dataset. For ablation studies, we use our “bracketed” dataset (see Section 3.2) as the training dataset.

Metrics We use common quantitative metrics: Peak Signal-To-Noise Ratio (PSNR) and Structural Similarity Image Metric (SSIM). High PSNR and SSIM scores indicate better quality.

5.1. Quantitative Comparisons

Medium Motion. Table 1 presents mid frame interpolation comparisons with DAIN [2], AdaCoF [15], BMBC [25], SoftSplat [21], and ABME [26] on small to medium motion datasets, namely Vimeo-90K [40], Middlebury [1], and UCF101 [18]. To make the comparisons fair and clear, we report results for each method trained with the Vimeo-90K dataset, which contains 51,313 triplets.

SoftSplat method reports two sets of results, one set trained with color loss (\mathcal{L}_{Lap}), which performs better on standard benchmarks, and another trained with a perceptually-sensitive loss (\mathcal{L}_F), which leads to perceptually higher quality frames. The rest reports results obtained by training with various color or low-level loss functions.

	Vimeo-90K [40]		Middlebury [1]		UCF101 [18]	
	PSNR↑	SSIM↑	PSNR↑	SSIM↑	PSNR↑	SSIM↑
DAIN	34.70	0.964	36.70	0.965	35.00	0.950
AdaCoF	34.35	0.973	35.72	0.978	34.90	0.968
BMBC	35.01	0.976	n/a	n/a	35.15	0.969
SoftSplat- \mathcal{L}_{Lap}	36.10	0.970	38.42	0.971	35.39	0.952
ABME	36.18	0.981	n/a	n/a	35.38	0.970
Our FILM- \mathcal{L}_1	36.06	0.970	37.52	0.966	35.32	0.952
SoftSplat- \mathcal{L}_F	35.48	0.964	37.55	0.965	35.10	0.948
Our FILM- \mathcal{L}_{VGG}	35.76	0.967	37.43	0.966	35.20	0.950
Our FILM- \mathcal{L}_S	35.87	0.968	37.57	0.966	35.16	0.949

Table 1. Comparison of video frame interpolation methods on *medium motion* benchmarks. The **blue** indicates best score for benchmark-focused losses, and **red** for perceptually-sensitive losses.

Based on color losses, ABME outperforms all other methods on Vimeo-90K, which contains 3,782 frame triplets. On Middlebury and UCF101, which contains 12 and 379 frame triplets, respectively, SoftSplat trained with

color loss has the highest PSNR. It is of note that ABME and SoftSplat are heavy networks. Each consists of multiple sub-networks dedicated for motion estimation, refinement or synthesis. Their training processes involve multiple datasets, stage-wise pre-training or fine-tuning. Our unified, single-stage, FILM network achieves competing PSNR scores.

The perception-distortion tradeoff [3] proved that minimizing distortion metrics alone, like PSNR or SSIM, can have a negative effect on the perceptual quality. The ultimate aim of frame interpolation research is to achieve low distortion, high perceptual quality and temporally coherent videos. As such, we also optimize our models with our proposed Gram Matrix-based loss, \mathcal{L}_S , which optimally favours both distortion and perceptual quality.

When including perceptually-sensitive losses, FILM outperforms the state-of-the-art SoftSplat on Vimeo-90K. We also achieve the highest scores on Middlebury and UCF101. In the next Subsection 5.2, we show visual comparisons that support the quantitative gains in PSNR with gains in image quality.

Large Motion. To compare FILM on large motion, we use the 4K samples in the Xiph benchmark [19]. Figure 3 shows motion magnitude histograms for Vimeo-90K and Xiph datasets. Vimeo-90K (3a) motion range is limited to 25 pixels, while the Xiph (3b) is characterized by a long-tailed distribution extending to 80 pixels. Following SoftSplat [21], we report results on Xiph_2K and Xiph_4K versions, each containing 392 triplets. The Xiph_2K version is obtained by down-sampling the original 4K samples by a factor of 2, while the Xiph_4K by a simple center-cropping to a 2K spatial size.

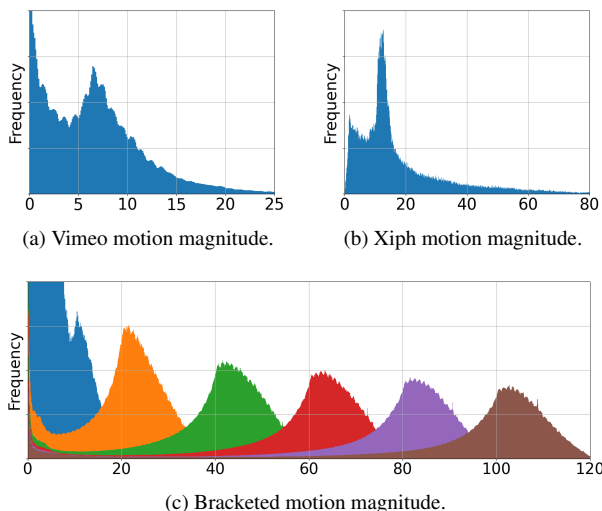


Figure 3. Motion magnitude histograms of datasets Vimeo-90K (3a), Xiph-4K (3b) and Bracketed (3c).

Table 2 presents mid frame interpolation comparisons on Xiph. Our FILM outperforms all other methods. For models trained with L1 color losses, we report two results, FILM- \mathcal{L}_1 trained with Vimeo-90K and another one trained with our custom large motion dataset. The first one outperforms all other Vimeo90K-trained models in both Xiph-2K and Xiph-4K whereas the latter provides a large 0.6 dB margin on Xiph-4K, the benchmark with the largest motions.

When including perceptually-sensitive losses, FILM again outperforms SoftSplat- \mathcal{L}_F . This demonstrates the generalization ability of FILM. We hope our findings would be interesting to the image synthesis research community, where large motion is often challenging. In the next Subsection 5.2, we provide visual results that support the effectiveness of our method in samples with motion ranges as large as 100 pixels.

	Xiph-2K [19]		Xiph-4K [19]	
	PSNR↑	SSIM↑	PSNR↑	SSIM↑
DAIN	35.95	0.940	33.49	0.895
ToFlow	33.93	0.922	30.74	0.856
AdaCoF	34.86	0.928	31.68	0.870
BMBC	32.82	0.928	31.19	0.880
ABME	36.53	0.944	33.73	0.901
SoftSplat- \mathcal{L}_{Lap}	36.62	0.944	33.60	0.901
Our FILM- \mathcal{L}_1	36.66	0.951	33.78	0.906
Our FILM- \mathcal{L}_1^1	36.41	0.948	34.25	0.909
SoftSplat- \mathcal{L}_F	35.74	0.944	32.55	0.865
Our FILM- \mathcal{L}_{VGG}	36.37	0.937	33.30	0.885
Our FILM- \mathcal{L}_S	36.38	0.942	33.29	0.882

Table 2. Comparison of video frame interpolation methods on *large motion* benchmarks. The **blue** indicates best score for benchmark-focused losses, and **red** for perceptually-sensitive losses.

5.2. Qualitative Comparisons

We provide visual results that support our quantitative results. We use the version of the model that yields high image quality, our FILM- \mathcal{L}_S and SoftSplat- \mathcal{L}_F . For ABME², we create visual results using the released pre-trained models. For SoftSplat³ [21], we use our faithful implementation, since neither source code nor pre-trained model was publicly available at the time of writing. Note that, SoftSplat³ provide only a CuPy implementation of the softmax splatting operator.

Sharpness. To evaluate the effectiveness of our Gram Matrix-based loss function (Equation 11) in preserving image sharpness, we visually compare our results against images rendered with other methods. Compared to the other

¹Trained with the large motion dataset as described in Section 3.2

²<https://github.com/JunHeum/ABME>

³<https://github.com/sniklaus/softmax-splatting>

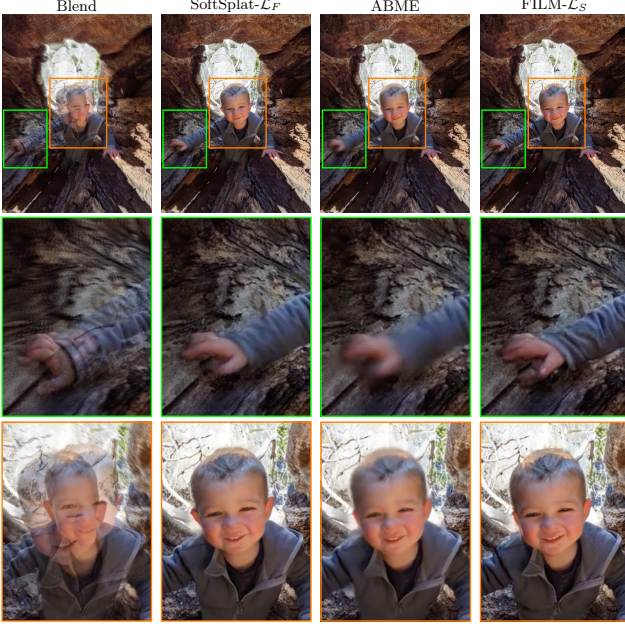


Figure 4. Comparison of frame interpolation methods on sharpness. Inputs overlaid (left), individual frames are available in the Supplementary materials. SoftSplat [21] shows artifacts (fingers) and ABME [26] show blurriness (the face). FILM produces sharp images and preserves the fingers.

approaches, as seen in Figure 4, our method synthesizes visually superior results, with crisp image details on the face and preserving the articulating fingers.

Disocclusion inpainting. In frame interpolation, most of the occluded pixels should be visible from the input frames. A fraction of the pixels, depending on the complexity or magnitude motion, could be unavailable from the inputs. Thus, to effectively inpaint the pixels, models must learn appropriate motions or hallucinate novel pixels. Figure 5 shows different methods, including ours, in-painting large dis-occlusions. Compared to the other approaches, FILM correctly paints the pixels while maintaining sharpness. It also preserves the structure of objects, e.g. the red toy car, while SoftSplat [21] shows deformation, and ABME [26] creates blurry in-painting.

Large Motion. Large motion is one of the most challenging aspects of frame interpolation. To account for the expanded motion search range, models often resort to multi-scale approaches or dense feature maps to increase the model’s neural capacity. Other approaches specialize models by training on large motion datasets. Figure 6 shows results for different methods on a sample with 100 pixels disparity. Both SoftSplat [21] and ABME [26] were able to capture motions near the dog’s nose, however they create large artifacts on the ground. FILM’s strength is seen capturing the motion well and keeping the background details.

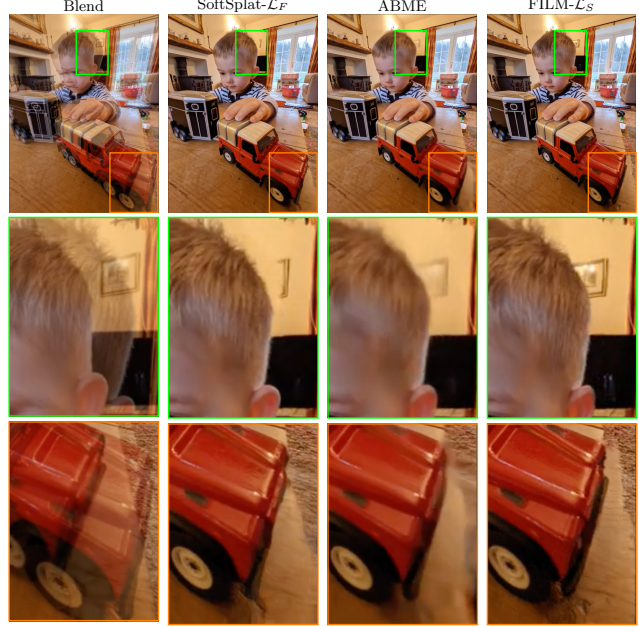


Figure 5. Qualitative results of disocclusion inpainting. Our method inpaints disocclusions well, and because of our Gram-Matrix-based loss, creates sharp image details, while SoftSplat [21] and ABME [26] produce blurry in-paintings or unnatural deformations.

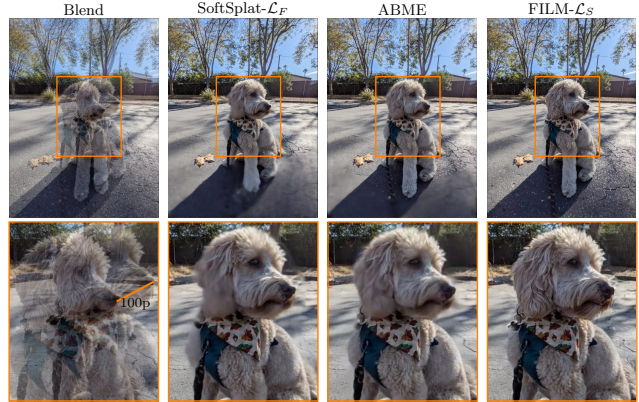


Figure 6. Comparison of frame interpolation on a large motion. Inputs with 100pixels disparity overlaid (left). Although both SoftSplat [21], ABME [26] capture the motion on the dog’s nose, they appear blurry, and create a large artifact on the ground. FILM’s strength is seen capturing the motion well and keeping the background details.

5.3. Ablations

In this section, we present ablation studies to analyze the design choices of FILM.

Weight Sharing. We compare our shared feature extractor with a regular UNet-like encoder [30], that uses independent weights at all scales, forcing us to also learn an independent flow predictor for each scale. Table 3 presents mid-

model	PSNR(w/ sharing)	PSNR (w/o sharing)
FILM	36.06	N/A
FILM-med	35.30	35.28
FILM-lite	35.09	34.93

Table 3. Weight sharing ablation study. A model without multi-scale feature sharing achieves results that are slightly lower than those achieved with shared features, e.g. FILM-med and FILM-lite. We have not been able to train our highest quality model (FILM) without weight sharing as the training gets unstable (indicated with N/A).



Figure 7. Loss function comparison on our FILM. \mathcal{L}_1 loss (left), \mathcal{L}_1 plus VGG loss (middle), and our proposed style loss (right), showing significant sharpness improvements (green box).

frame results in PSNR. It is not straightforward to construct models that are fair to compare: one could either match the total number of weights or the number of filters at each level. We chose to use a UNet encoder that starts from the same number of filters as ours and then doubles the number at each level. The FILM-model we have used in this paper starts with 64 filters, so this leads to a UNet with feature counts: [64, 128, 256...]. We find that training with this configuration does not converge without weight sharing. To study this further, we construct two simpler variants of our model, starting from 32 filters. We are able to train these two models with just a small loss in PSNR as compared to the equivalent model that shares weights.

To conclude, weight sharing allows training a more powerful model, reaching a higher PSNR. Additionally, sharing may be important for fitting models in GPU memory in practical applications.

Gram Matrix (Style) Loss. Figure 7 presents qualitative results of FILM trained with \mathcal{L}_1 , adding \mathcal{L}_{VGG} , and with our proposed style loss \mathcal{L}_S , given by Equation 12. Using \mathcal{L}_1 alone leads to blurry images (red box), while adding \mathcal{L}_{VGG} loss reduces blurry artifacts (orange box). Our proposed loss (green box) significantly improves sharpness of our FILM method.

Motion Ranges. We study the effect of the training dataset’s motion range on the model’s ability to handle different motions at test time. For this study, we use a reduced FILM-med to save compute resources. We conduct our study using the motion “bracketed” dataset (see Section 3.2). FILM-

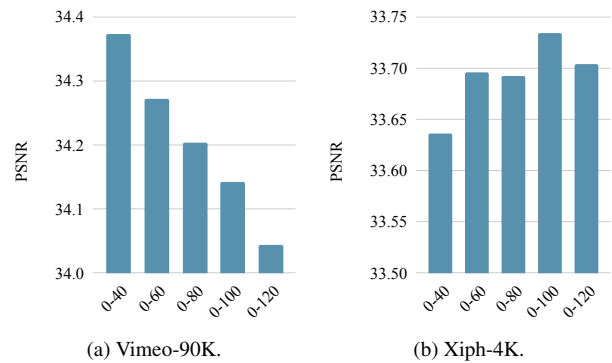


Figure 8. A study of the effect of the training dataset’s motion range on the PSNR, when evaluated on Vimeo-90K (8a), and Xiph-4K (8b). Motion distribution of the evaluation datasets are shown in Figure 3. We use a reduced FILM-med model to save compute resources.

med is trained on motion ranges of 0-40, 0-60, 0-80, 0-100 and 0-120 pixels. They are evaluated on Vimeo-90K (0-25 range) and Xiph4K (0-80 range), as shown in Figure 8.

On Vimeo-90K, FILM-med trained with the smallest motion range performs the best. As larger motion is added, PSNR goes down significantly. We hypothesize that this behavior is caused by two factors: 1) when training for larger motion, the model assumes a larger search window for correspondence, and thus has more chances to make errors. 2) with larger motion, the problem is simply harder and less neural capacity is left for smaller motion.

On Xiph-4K, the best performance is obtained by training with motion range 0-100 pixels. Motivated by our finding, we trained our best model (FILM) with this dataset, and show in Table 2 that we achieve a PSNR improvement of +0.5dB over the state-of-the-art.

In summary, our findings indicate that scale-agnostic features and shared weight flow prediction improve the model’s ability to learn and generalize to a wider range of motion. In addition, we find that best results are obtained when the training data also matches the test-time motion distribution.

5.4. Limitations

In some instances, FILM produces un-natural deformations when the in-between motion is extreme. While the resulting videos are appealing, the subtle movements may not look natural. We provide example videos in our GitHub code release.

6. Conclusions

We present a robust algorithm for large motion frame interpolation (FILM). FILM is trainable from frame triplets alone and does not depend on additional optical-flow or depth priors. We propose an effective multi-scale feature

extractor to learn bi-directional motion in a scale-agnostic manner, that generalizes well to large motion. We optimize our models with the Gram matrix loss that matches the correlation of feature maps to synthesize high quality frames. To the best of our knowledge, this is the first work that utilizes shared feature extraction and Gram matrix loss for frame interpolation. Our method outperforms other methods and handles large motion well. Future work will study the utility of our shared feature extractor for other image synthesis tasks. Source code of FILM can be found at <https://github.com/google-research/frame-interpolation>.

Acknowledgements.: We thank Orly Liba for feedback on the text, Jamie Aspinall for the imagery in the paper, Dominik Kaeser, Yael Pritch, Michael Nechyba and David Salesin for support.

References

- [1] Simon Baker, Daniel Scharstein, JP Lewis, Stefan Roth, Michael J Black, and Richard Szeliski. A database and evaluation methodology for optical flow. *International journal of computer vision*, 92(1):1–31, 2011. [2](#) [5](#)
- [2] Wenbo Bao, Wei-Sheng Lai, Chao Ma, Xiaoyun Zhang, Zhiyong Gao, and Ming-Hsuan Yang. Depth-aware video frame interpolation. In *Proceedings of the IEEE/CVF Conference on Computer Vision and Pattern Recognition*, pages 3703–3712, 2019. [2](#) [5](#)
- [3] Yochai Blau and Tomer Michaeli. The perception-distortion tradeoff. In *Proceedings of the IEEE Conference on Computer Vision and Pattern Recognition*, pages 6228–6237, 2018. [6](#)
- [4] Léon Bottou. Stochastic gradient descent tricks. In *Neural networks: Tricks of the trade*, pages 421–436. Springer, 2012. [2](#)
- [5] Tim Brooks and Jonathan T Barron. Learning to synthesize motion blur. In *Proceedings of the IEEE/CVF Conference on Computer Vision and Pattern Recognition*, pages 6840–6848, 2019. [4](#)
- [6] Tianyu Ding, Luming Liang, Zhihui Zhu, and Ilya Zharkov. Cdfi: Compression-driven network design for frame interpolation. In *Proceedings of the IEEE/CVF Conference on Computer Vision and Pattern Recognition*, pages 8001–8011, 2021. [2](#)
- [7] Alexey Dosovitskiy and Thomas Brox. Generating images with perceptual similarity metrics based on deep networks. *Advances in neural information processing systems*, 29:658–666, 2016. [4](#)
- [8] Leon A Gatys, Alexander S Ecker, and Matthias Bethge. Image style transfer using convolutional neural networks. In *Proceedings of the IEEE conference on computer vision and pattern recognition*, pages 2414–2423, 2016. [2](#) [4](#)
- [9] Junhwa Hur and Stefan Roth. Iterative residual refinement for joint optical flow and occlusion estimation. In *Proceedings of the IEEE/CVF Conference on Computer Vision and Pattern Recognition*, pages 5754–5763, 2019. [2](#)
- [10] Huaiyu Jiang, Deqing Sun, Varun Jampani, Zhaoyang Lv, Erik Learned-Miller, and Jan Kautz. Sense: A shared encoder network for scene-flow estimation. In *Proceedings of the IEEE/CVF International Conference on Computer Vision*, pages 3195–3204, 2019. [2](#)
- [11] Huaiyu Jiang, Deqing Sun, Varun Jampani, Ming-Hsuan Yang, Erik Learned-Miller, and Jan Kautz. Super slomo: High quality estimation of multiple intermediate frames for video interpolation. In *Proceedings of the IEEE Conference on Computer Vision and Pattern Recognition*, pages 9000–9008, 2018. [2](#)
- [12] Tero Karras, Miika Aittala, Samuli Laine, Erik Härkönen, Janne Hellsten, Jaakko Lehtinen, and Timo Aila. Alias-free generative adversarial networks. In *Proc. NeurIPS*, 2021. [2](#)
- [13] AdamJB KingaD. A methodforstochasticoptimization. *Anon. International Conference on Learning Representations. SanDego: ICLR*, 2015. [5](#)
- [14] Christian Ledig, Lucas Theis, Ferenc Huszár, Jose Caballero, Andrew Cunningham, Alejandro Acosta, Andrew Aitken, Alykhan Tejani, Johannes Totz, Zehan Wang, et al. Photo-realistic single image super-resolution using a generative adversarial network. In *Proceedings of the IEEE conference on computer vision and pattern recognition*, pages 4681–4690, 2017. [4](#)
- [15] Hyeongmin Lee, Taeoh Kim, Tae-young Chung, Daehyun Pak, Yuseok Ban, and Sangyoun Lee. Adacof: Adaptive collaboration of flows for video frame interpolation. In *Proceedings of the IEEE/CVF Conference on Computer Vision and Pattern Recognition*, pages 5316–5325, 2020. [2](#) [5](#)
- [16] Guilin Liu, Fitzsum A Reda, Kevin J Shih, Ting-Chun Wang, Andrew Tao, and Bryan Catanzaro. Image inpainting for irregular holes using partial convolutions. In *Proceedings of the European Conference on Computer Vision (ECCV)*, pages 85–100, 2018. [4](#)
- [17] Yu-Lun Liu, Yi-Tung Liao, Yen-Yu Lin, and Yung-Yu Chuang. Deep video frame interpolation using cyclic frame generation. In *Proceedings of the AAAI Conference on Artificial Intelligence*, pages 8794–8802, 2019. [2](#)
- [18] Ziwei Liu, Raymond A Yeh, Xiaou Tang, Yiming Liu, and Aseem Agarwala. Video frame synthesis using deep voxel flow. In *Proceedings of the IEEE International Conference on Computer Vision*, pages 4463–4471, 2017. [2](#) [5](#)
- [19] Chris Montgomery et al. Xiph. org video test media (derf’s collection), the xiph open source community, 1994. *Online*, <https://media.xiph.org/video/derf>, 3, 1994. [5](#) [6](#)
- [20] Simon Niklaus and Feng Liu. Context-aware synthesis for video frame interpolation. In *Proceedings of the IEEE conference on computer vision and pattern recognition*, pages 1701–1710, 2018. [2](#)
- [21] Simon Niklaus and Feng Liu. Softmax splatting for video frame interpolation. In *Proceedings of the IEEE/CVF Conference on Computer Vision and Pattern Recognition*, pages 5437–5446, 2020. [1](#) [2](#) [5](#) [6](#) [7](#)
- [22] Simon Niklaus, Long Mai, and Feng Liu. Video frame interpolation via adaptive convolution. In *Proceedings of the IEEE Conference on Computer Vision and Pattern Recognition*, pages 670–679, 2017. [2](#)

[23] Simon Niklaus, Long Mai, and Feng Liu. Video frame interpolation via adaptive separable convolution. In *Proceedings of the IEEE International Conference on Computer Vision*, pages 261–270, 2017. 2, 4

[24] Simon Niklaus, Long Mai, and Oliver Wang. Revisiting adaptive convolutions for video frame interpolation. In *Proceedings of the IEEE/CVF Winter Conference on Applications of Computer Vision*, pages 1099–1109, 2021. 2

[25] Junheum Park, Keunsoo Ko, Chul Lee, and Chang-Su Kim. Bmbc: Bilateral motion estimation with bilateral cost volume for video interpolation. In *Computer Vision–ECCV 2020: 16th European Conference, Glasgow, UK, August 23–28, 2020, Proceedings, Part XIV 16*, pages 109–125. Springer, 2020. 2, 5

[26] Junheum Park, Chul Lee, and Chang-Su Kim. Asymmetric bilateral motion estimation for video frame interpolation. In *Proceedings of the IEEE/CVF International Conference on Computer Vision*, pages 14539–14548, 2021. 1, 2, 5, 7

[27] Federico Perazzi, Jordi Pont-Tuset, Brian McWilliams, Luc Van Gool, Markus Gross, and Alexander Sorkine-Hornung. A benchmark dataset and evaluation methodology for video object segmentation. In *Proceedings of the IEEE conference on computer vision and pattern recognition*, pages 724–732, 2016. 1, 5

[28] Fitsum A Reda, Guilin Liu, Kevin J Shih, Robert Kirby, Jon Barker, David Tarjan, Andrew Tao, and Bryan Catanzaro. Sdc-net: Video prediction using spatially-displaced convolution. In *Proceedings of the European Conference on Computer Vision (ECCV)*, pages 718–733, 2018. 4

[29] Fitsum A Reda, Deqing Sun, Aysegul Dundar, Mohammad Shoeybi, Guilin Liu, Kevin J Shih, Andrew Tao, Jan Kautz, and Bryan Catanzaro. Unsupervised video interpolation using cycle consistency. In *Proceedings of the IEEE/CVF International Conference on Computer Vision*, pages 892–900, 2019. 2

[30] Olaf Ronneberger, Philipp Fischer, and Thomas Brox. U-net: Convolutional networks for biomedical image segmentation. In *International Conference on Medical image computing and computer-assisted intervention*, pages 234–241. Springer, 2015. 3, 7

[31] Mehdi SM Sajjadi, Bernhard Scholkopf, and Michael Hirsch. Enhancenet: Single image super-resolution through automated texture synthesis. In *Proceedings of the IEEE International Conference on Computer Vision*, pages 4491–4500, 2017. 4

[32] Hyeyonjun Sim, Jihyong Oh, and Munchurl Kim. Xvfi: Extreme video frame interpolation. In *Proceedings of the IEEE/CVF International Conference on Computer Vision*, pages 14489–14498, 2021. 2

[33] Karen Simonyan and Andrew Zisserman. Very deep convolutional networks for large-scale image recognition. *arXiv preprint arXiv:1409.1556*, 2014. 4

[34] Deqing Sun, Xiaodong Yang, Ming-Yu Liu, and Jan Kautz. PWC-Net: CNNs for optical flow using pyramid, warping, and cost volume. In *CVPR*, June 2018. 2, 3

[35] Carlo Tomasi and Takeo Kanade. Detection and tracking of point features. *Carnegie Mellon University Technical Report CMU-CS-91-132*, April 1991. 5

[36] Quang Nhat Tran and Shih-Hsuan Yang. Efficient video frame interpolation using generative adversarial networks. *Applied Sciences*, 10(18):6245, 2020. 2

[37] Marc Comino Trinidad, Ricardo Martin Brualla, Florian Kainz, and Janne Kontkanen. Multi-view image fusion. In *Proceedings of the IEEE/CVF International Conference on Computer Vision*, pages 4101–4110, 2019. 2, 3, 4

[38] Joost van Amersfoort, Wenzhe Shi, Alejandro Acosta, Francisco Massa, Johannes Totz, Zehan Wang, and Jose Caballero. Frame interpolation with multi-scale deep loss functions and generative adversarial networks. *arXiv preprint arXiv:1711.06045*, 2017. 2

[39] Xiaoyu Xiang, Yapeng Tian, Yulun Zhang, Yun Fu, Jan P Allebach, and Chenliang Xu. Zooming slow-mo: Fast and accurate one-stage space-time video super-resolution. In *Proceedings of the IEEE/CVF conference on computer vision and pattern recognition*, pages 3370–3379, 2020. 2

[40] Tianfan Xue, Baian Chen, Jiajun Wu, Donglai Wei, and William T Freeman. Video enhancement with task-oriented flow. *International Journal of Computer Vision*, 127(8):1106–1125, 2019. 2, 3, 5

FILM: Frame Interpolation for Large Motion

Supplementary Material

A. Details of Network Architecture

Table 4 presents FILM’s network architecture details.

Convolutional Layer Name	Filter Size	# Input Filters	# Output Filters
FeatExtr_shared_1_1	3×3	3	64
FeatExtr_shared_1_2	3×3	64	64
FeatExtr_shared_2_1	3×3	64	128
FeatExtr_shared_2_2	3×3	128	128
FeatExtr_shared_3_1	3×3	128	256
FeatExtr_shared_3_2	3×3	256	256
FeatExtr_shared_4_1	3×3	256	512
FeatExtr_shared_4_2	3×3	512	512
FlowPred_1_1	3×3	128	32
FlowPred_1_2	3×3	32	32
FlowPred_1_3	3×3	32	32
FlowPred_1_4	1×1	32	16
FlowPred_1_5	1×1	16	2
FlowPred_2_1	3×3	384	64
FlowPred_2_2	3×3	64	64
FlowPred_2_3	3×3	64	64
FlowPred_2_4	1×1	64	32
FlowPred_2_5	1×1	32	2
FlowPred_3_1	3×3	896	128
FlowPred_3_2	3×3	128	128
FlowPred_3_3	3×3	128	128
FlowPred_3_4	1×1	128	64
FlowPred_3_5	1×1	64	2
FlowPred_shared_1	3×3	1920	256
FlowPred_shared_2	3×3	256	256
FlowPred_shared_3	3×3	256	256
FlowPred_shared_4	1×1	256	128
FlowPred_shared_5	1×1	128	2
Fusion_1	2×2	128	64
Fusion_2	3×3	202	64
Fusion_3	3×3	64	64
Fusion_4	3×3	256	128
Fusion_5	2×2	522	128
Fusion_6	3×3	128	128
Fusion_7	2×2	512	256
Fusion_8	3×3	1162	256
Fusion_9	3×3	256	256
Fusion_10	2×2	1930	512
Fusion_11	3×3	2442	512
Fusion_12	3×3	512	512
Final_Conv	1×1	64	3

Table 4. FILM network details. Each convolution module has a bias and a ReLU non-linearity. All spatial down- and up-sampling are done using an AveragePooling2D and an UpSampling2D layer with bilinear mode, and a factor of 2.

B. Memory and Compute

Table 5 presents inference times and memory comparisons on a V100 GPU. Our FILM is $3.21 \times$ faster than ABME, and $10 \times$ faster than SoftSplat, while using only $1.22 \times$ and $1.67 \times$ more memory than ABME and SoftSplat,

respectively. Our model is somewhat larger due to its deep pyramid (7 levels), but the time performance gains are significantly larger still.

Interpolation Method	Inference Time (second)↓	Peak Memory (GB)↓
SoftSplat ⁴	8.03	5.399
ABME ⁵	2.58	7.392
Our FILM	0.804	9.029

Table 5. Memory and compute performance for a 2048×1024 frame interpolation. We report the average of 10 runs.

⁴Obtained with our implementation.

⁵Obtained with <https://github.com/JunHeum/ABME>.